


NANO EXPRESS

Open Access

Observation of Landau Level-Dependent Aharonov-Bohm-Like Oscillations in a Topological Insulator

Shiu-Ming Huang^{1,2*} , Chien Lin¹, Sheng-Yu You¹, Pin-Cyuan Chen¹, Jai-Long Hong¹, Jyun-Fong Wong¹, You-Jhih Yan³, Shih-Hsun Yu³ and Mitch M. C. Chou^{2,3}

Abstract

We study the quantum oscillations in the BiSbTe₃ topological insulator. In addition to the Shubnikov-de Haas (SdH) oscillation, the Aharonov-Bohm-like (ABL) oscillations are also observed. The ABL oscillation period is constant at each Landau level (LL) which is determined from the SdH oscillation. The shorter ABL oscillation periods are observed at lower LLs. The oscillation period is proportional to the square root of the LL at temperatures. The ratio of the ABL oscillation period to the effective mass is weak LL dependence. The LL-dependent ABL oscillation might originate from the LL-dependent effective mass.

Keywords: Aharonov-Bohm-like oscillations, Shubnikov-de Haas oscillation, Landau level

Introduction

Aharonov-Bohm (AB) interference originates from the carrier wavefunction interference in a loop which might be patterned ring [1, 2], material geometric structure [3–6, 8–11], or carrier transport trajectory [12]. The magnetic field, B , through the loop will induce carrier wavefunction phase shift that leads to periodic wavefunction interference oscillations. This oscillation period is sensitive to the carrier transport characteristics, such as carrier coherence length and mobility [3, 12]. The quantum interference is an excellent tool to detect material transport characteristics and understand intrinsic mechanisms. Due to the short carrier coherence length and the small flux quantum, the quantum interference is mainly reported at high mobility nanowires or patterned nano-rings at low B [3–6, 8–11]. Reports on a macroscopic system at high B are rare. The works on AB quantum interference at high

B are less investigated, and the related mechanism is less understood.

In this work, quantum oscillations were performed in a BiSbTe₃ topological insulator macroflake at high B . In addition to the Shubnikov-de Haas (SdH) oscillation, the Aharonov-Bohm-like (ABL) oscillation was observed. The ABL oscillation period is B -dependent and is different from the traditional AB oscillation, which the oscillation period is independent of B . The observed ABL oscillation period is constant at each Landau level (LL), which is determined from the SdH oscillation. The shorter oscillation periods are observed at lower LLs. The oscillation period is proportional to the square root of the LL at temperatures. The ratio of the ABL oscillation period to the effective mass is weak LL dependence. The LL-dependent ABL oscillation might originate from the LL-dependent effective mass.

Experimental Method

The growth condition of the BiSbTe₃ single crystal is the same as our previous work on the topological insulators [13–16]. Our previous work demonstrated that TI with extremely high uniformity can be obtained using the

*Correspondence: smhuang@mail.nsysu.edu.tw

¹Department of Physics, National Sun Yat-Sen University, 80424 Kaohsiung, Taiwan

²Taiwan Consortium of Emergent Crystalline Materials, TCECM, National Sun Yat-Sen University, 80424 Kaohsiung, Taiwan

Full list of author information is available at the end of the article

RHFZ method [13–16]. Raman, EDS, and XPS spectrum proved that the crystal is BiSbTe₃. The BiSbTe₃ single crystal flakes were obtained using the Scotch-tape method. The cleaved flake geometry is roughly 3 mm in length, 2 mm in width, and 170 μm in thickness. Magnetotransport measurements were performed using the standard six-probe technique in a commercial apparatus (Quantum Design PPMS) with a B of up to 14 T. The B was applied perpendicular to the large cleaved surface. The data points are taken per 100 Gauss at magnetic field region between 6 and 14 T in the steady magnetic field mode, instead of the sweeping magnetic field mode.

Results and Discussion

Figure 1 shows the magnetoresistances (MRs) as a function of B . The $R(14\text{T})/R(0\text{T})$ reaches 10 and is higher than most reported values in Bi_{*x*}Sb_{*2-x*}Te_{*y*}Se_{*3-y*} topological insulators [17–23, 23–33]. Both theoretical and experimental investigations support that the MR ratio is proportional to the carrier mobility [34]. The measured high MR ratio supports the high quality of our BiSbTe₃ sample. The top-left inset reveals the dR/dB as a function of $1/B$. It reveals that periodic oscillations and oscillation peaks and dips are at the same B at 2 and 8 K. This is known as SdH oscillation that originates from a two-dimensional system. The SdH oscillation period corresponds to the Fermi momentum vector, k_f . The bottom-right inset shows the fast Fourier transform (FFT) of the SdH oscillation. A

sharp peak at 48 T is observed for both 2 and 8 K. Following the Onsager relation, one could estimate k_f through $F = \frac{\hbar k_f^2}{2e}$, where F is the SdH oscillation frequency. The $F = 48\text{ T}$ leads to the $k_f = 3.8\text{ \AA}^{-1}$, which is consistent with the observed value from ARPES from a different batch of the same crystal and from reported values in literature [35]. That supports the high quality and uniformity of our BiSbTe₃ crystal. As well as the SdH oscillation, the top-left inset reveals oscillations with a short period. To suppress the influence of the SdH oscillation and extract oscillation characteristics, the d^2R/dB^2 is performed.

Figure 2 exhibits the dR/dB and d^2R/dB^2 as a function of B at 2 and 8 K. Dot lines label oscillation peaks in d^2R/dB^2 , and long dash lines correspond to B of LLs that are determined from the extracted SdH oscillation frequency. The periodic oscillations is similar to the AB oscillation. The AB oscillation period is expressed as $\Delta B = \frac{\Phi}{A}$. Φ is the flux quantum, where $\frac{h}{e}$, and A is the geometry area looped by clock-count and anti-clock-count carrier trajectories in a confined structure. Due to the small flux quantum, the AB oscillation is mainly observed in confinement by artificial nanostructures [1, 2], such as nano-rings and nanowires [3–11]. Recently, it is reported that carrier elastic scattering trajectory might form a series of connected closed loops in a macroscopic system. A B flux through these loops would induce carrier wavefunction phase shift and lead to periodic ABL

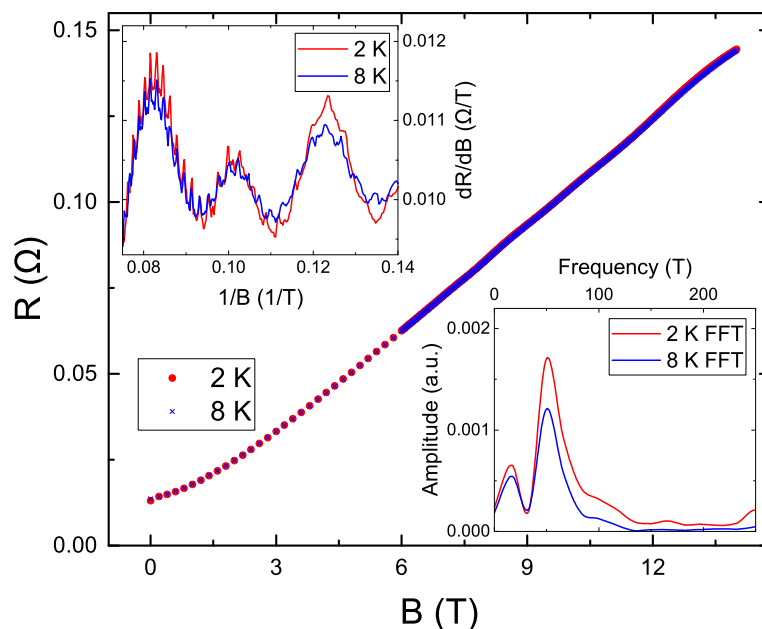


Fig. 1 The magnetoresistance as a function of magnetic fields at 2 and 8 K. The top-left inset shows the dR/dB as a function of inverse magnetic fields. It reveals periodic oscillations. The bottom-right inset shows the fast Fourier transform of the SdH oscillation and a sharp peak at 48 T for both 2 and 8 K

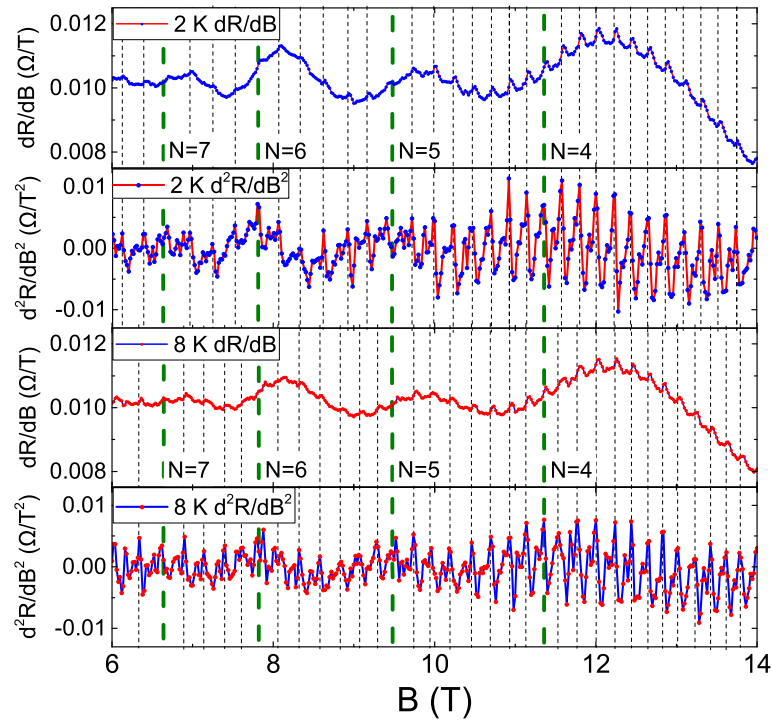


Fig. 2 The dR/dB and d^2R/dB^2 as a function of B at 2 and 8 K. It shows periodic oscillations and the oscillation period is Landau level dependence

oscillations [12]. The extracted elastic scattering length is roughly 150 nm which corresponds to the oscillation period with 0.02 T and is consistent with our experimental observation.

Following the dot lines in Fig. 2, one could note that the oscillation period is constant at each LL and the oscillation period is shorter at lower LLs. This behavior is different from the traditional AB oscillation. To extract and determine these oscillation periods, FFT is performed at different LLs. Figure 3 shows the FFT at different LLs at 2 and 8 K, and it clearly reveals the higher oscillation frequency at lower LLs at 2 and 8 K.

A similar LL-dependent ABL oscillation is reported at the integer quantum Hall regime in semiconductor two-dimensional electron gas [36, 37]. It has been interpreted either as constructive interference of one-dimensional electron traveling along edge channels or as quantum wave interference of edge electrons. The carrier transport path in different edge channels leads to different effective areas in a confined pattern and eventually to different ABL oscillation periods in edge channels at different LLs [38–40]. Further studies on electric Fabry-Perot interferometers in integer and fractional quantum Hall regime reveal that the ABL oscillation period is related to the flux period by $\frac{\Phi}{f}$, where f is the fully occupied LL in the constrictions. The oscillation period is expected to be $\frac{\Phi}{Af}$, where A is the geometry area of the confined shape [41, 42].

Table 1 lists the extracted oscillation periods from the FFT at different LLs and temperatures. The analysis reveals that the ratio of the oscillation period to the square root of LL is constant at each temperature. This is different from the behavior of Fabry-Perot interferometer in which the oscillation is inversely proportional to LLs [41, 42]. On the other hand, the electric Fabry-Perot interference originates from carrier trajectory coupling between different LLs from inside and outside a confined pattern [37]. The oscillation is strongly related to the patterned geometry. There are no artificial patterns on the surface of our samples, and there should be no suitable coupling channels between different LLs. Furthermore, the geometry sizes of our samples are in the millimeter scale and the related AB oscillation period would be too small to be detected. Despite these differences from existing works, we think that aside from the geometric area and carrier coherence length, the intrinsic carrier characteristic might play a critical role on the LL-dependent ABL oscillation [3, 43].

Following the Lifshitz-Kosevich (LK) theory, one can extract characteristic parameters of the transport carriers in the surface state of the topological insulator, and the temperature dependence of the amplitude of the SdH oscillation is expressed as

$$\Delta R_{xx}(T, B) \propto \frac{\lambda(T/B)}{\sinh(\lambda(T/B))},$$

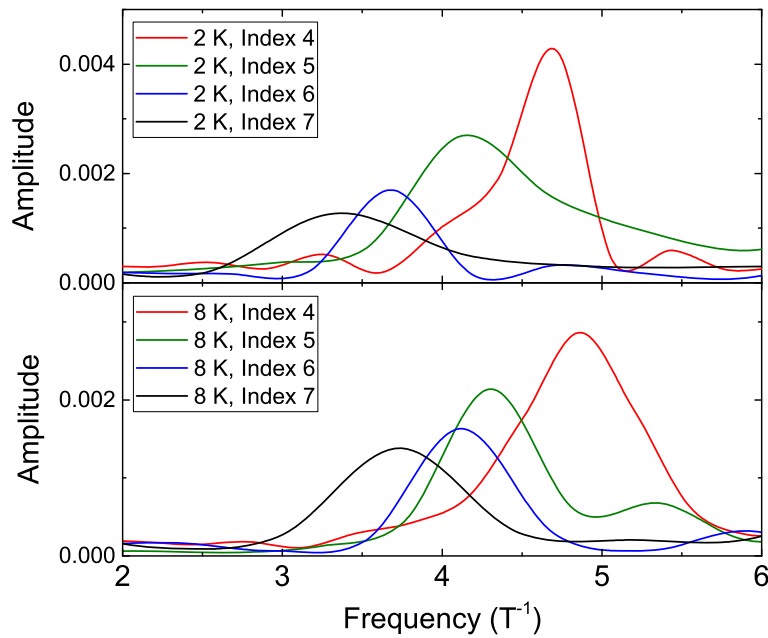


Fig. 3 The fast Fourier transform of the dR/dB at different Landau levels and temperatures. The higher oscillation frequency peak is observed at lower Landau levels

where $\lambda(T/B) = (2\pi^2 k_B T m_{cyc}) / (\hbar e B)$. Figure 4 shows the extracted normalized SdH oscillation amplitude as a function of temperature at different LLs. It agrees well with the LK theory and reveals different tendencies at different LLs. The fitting results support that the $m_{cyc} = 0.152m_0, 0.170m_0, 0.185m_0,$ and $0.191m_0$, where m_0 is the free electron mass, for $N = 4, 5, 6$ and 7 , respectively. These values are consistent with the reported effective masses in topological insulators [21, 22]. This Landau level-dependent effective mass is recently observed in the 3D Dirac semimetal $ZrTe_5$ [44]. However, the origin of the magnetic field-dependent effective mass is not clear yet. It needs further study to clarify the intrinsic mechanism.

The different effective mass would directly deviate the intrinsic carrier transport characteristic at Fermi surface, such as Fermi velocity, which is directly related to the carrier phase coherence length. The higher effective mass would lead to lower coherence length that corresponds to the longer AB-like oscillation period. This is qualitatively consistent with our experimental observation. As shown in Table 1, the ratio of the AB-like oscillation period to the effective mass shows weak LL dependence.

Table 1 List of the extracted oscillation period at different Landau levels and temperatures

Landau level N	Oscillation period (T) OP	OP/\sqrt{N}	$OP/m_{cyc} (T/m_0)$
4 (2 K)	0.215	0.107	1.41
5 (2 K)	0.235	0.105	1.38
6 (2 K)	0.260	0.106	1.40
7 (2 K)	0.284	0.107	1.45
4 (8 K)	0.206	0.103	1.35
5 (8 K)	0.233	0.104	1.37
6 (8 K)	0.249	0.101	1.34
7 (8 K)	0.260	0.098	1.36

The oscillation period is proportional to the square root of Landau level

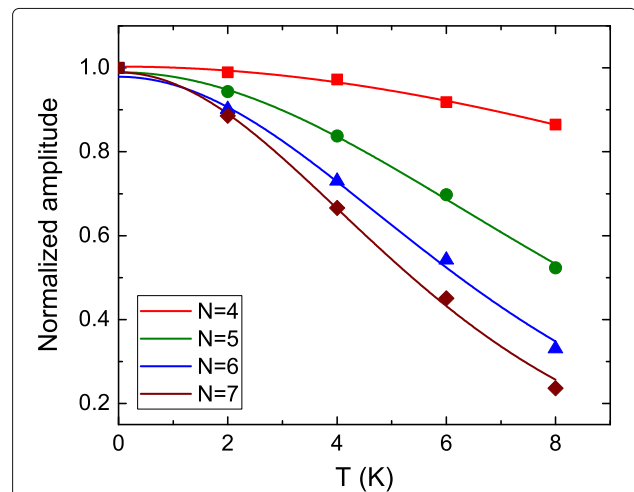


Fig. 4 The extracted normalized SdH oscillation amplitude as a function of temperature at different Landau levels. It agrees well with the LK theory and reveals different tendency at different Landau levels

The Landau level-dependent effective mass might be one of the intrinsic effects that leads to the LL-dependent oscillation period.

LL is a transport characteristic of a two-dimensional system. It indicates that the LL-dependent oscillation might have originated from the surface state carrier in TIs. Berry phase is a characteristic of transport carriers. Extracting the Berry phase might help identify the source of these LL-dependent periodic AB oscillations. We define the AB oscillation index number by dividing the corresponding B of oscillation peaks in dB/dB by the related oscillation period in the LL. It reveals that the index number of oscillation peaks in dB/dB corresponds to $N + 0.25$, where N is integer, for all oscillations in different LLs and temperatures. This further supports that the AB oscillation period is related to LLs. Figure 5 shows that AB oscillation index numbers are proportional to B at different LLs and temperatures. The intercept is 0.25 which indicates a 0.5 phase shift in the plot of the AB oscillation. This supports the Berry phase is π and the observed AB oscillations might be the carrier transport characteristic of the surface state in our BiSbTe₃ topological insulator [45].

Conclusion

We have reported the quantum oscillations in a BiSbTe₃ topological insulator macroflake. In addition to the Shubnikov-de Haas (SdH) oscillation, it reveals Aharonov-Bohm-like (ABL) oscillation. The ABL oscillation period is B -dependent. The ABL oscillation period is constant at each Landau level (LL). The shorter oscillation periods were observed at lower LLs, which was determined through the SdH oscillation. The oscillation period is proportional to the square root of the LL at

different temperatures. The ratio of the ABL oscillation period to the effective mass is weak LL dependence. The LL-dependent ABL oscillation might originate from the LL-dependent effective mass.

Abbreviations

EDS: Energy-dispersive X-ray spectroscopy. XPS: X-ray photoelectron spectroscopy. ARPES: Angle resolved photoemission spectroscopy. SdH: Shubnikov-de Haas

Authors' Contributions

SMH conceived the idea, analyzed these experimental results, and prepared the paper. CL, SYY, PCC, JLH, and JFW performed the experiments. YJY, SHY, and M.M.C.C. grow the high-quality crystal. The author(s) read and approved the final manuscript.

Funding

The work was supported by the Taiwan National Science Council through Grant Nos. MOST 106-2112-M-110-002 and MOST 107-2112-M-110-011-MY2, and Center of Crystal Research at National Sun Yat-Sen University. SMH thanks the support of the short-term overseas research for scientist and technician from the Taiwan National Science Council.

Availability of Data and Materials

The datasets generated during and/or analyzed during the current study are available from the corresponding authors on reasonable request.

Ethics Approval and Consent to Participate

All authors agreed on the ethics approval and consent to participate.

Competing Interests

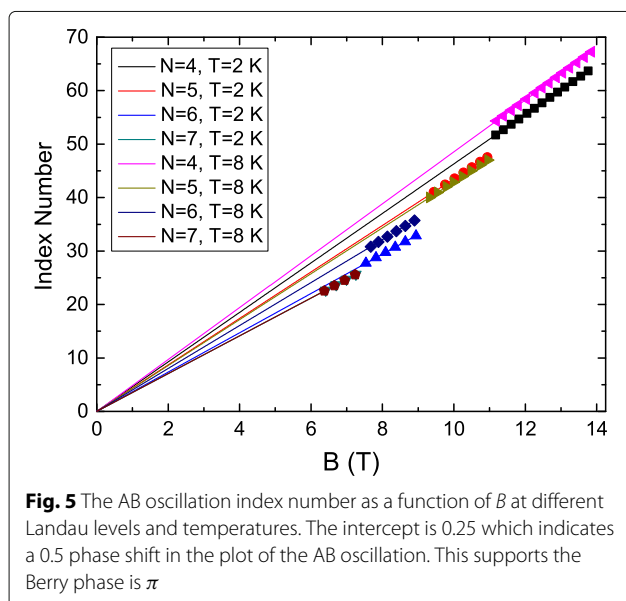
The authors declare that they have no competing interests.

Author details

¹Department of Physics, National Sun Yat-Sen University, 80424 Kaohsiung, Taiwan. ²Taiwan Consortium of Emergent Crystalline Materials, TCECM, National Sun Yat-Sen University, 80424 Kaohsiung, Taiwan. ³Department of Materials and Optoelectronic Science, National Sun Yat-Sen University, 80424 Kaohsiung, Taiwan.

Received: 31 January 2020 Accepted: 23 July 2020

Published online: 26 August 2020



References

- Webb RA, Washburn S, Umbach CP, Laibowitz RB (1985) Observation of $\frac{h}{e}$ Aharonov-Bohm Oscillations in Normal-Metal Rings. *Phys Rev Lett* 54:2696–2699
- Tomomura Akira, Osakabe Nobuyuki, Matsuda Tsuyoshi, Kawasaki Takeshi, Endo Junji, Yano Shinichiro, Yamada Hiroji (1986) Evidence for Aharonov-Bohm effect with magnetic field completely shielded from electron wave. *Phys Rev Lett* 56:792–795
- Dauber Jan, Oellers Martin, Venn Florian, Epping Alexander, Watanabe Kenji, Taniguchi Takashi, Hassler Fabian, Stampfer Christoph (2017) Aharonov-Bohm oscillations and magnetic focusing in ballistic graphene rings. *Phys Rev B* 96:205407-1–205407-13
- Wang LX, Li CZ, Yu DP, Liao ZM (2016) Aharonov–Bohm oscillations in Dirac semimetal Cd₃As₂ nanowires. *Nat Commun* 7:10769-1-10769-7
- Cho Sungjae, Dellabetta Brian, Zhong Ruidan, Schneeloch John, Liu Tiansheng, Gu Genda, Gilbert MatthewJ, Mason Nadya (2015) Aharonov–Bohm oscillations in a quasi-ballistic three-dimensional topological insulator nanowire. *Nat Commun* 6:7634-1-7634-5
- Xiu Faxian, He Liang, Wang Yong, Cheng Lina, Chang Li-Te, Lang Murong, Huang Guan, Kou Xufeng, Zhou Yi, Jiang Xiaowei, Chen Zhigang, Zou Jin, Shailos Alexandros, Wang KangL (2011) Manipulating surface states in topological insulator nanoribbons. *Nat Nanotechnol* 6:216–221
- Peng H, et al. (2010) Aharonov–Bohm interference in topological insulator nanoribbons. *Nat Mater* 9:225–229
- Hamdou B, Gooth J, Dorn A, Pippel E, Nielsch K (2013) Aharonov-Bohm oscillations and weak antilocalization in topological insulator Sb₂Te₃ nanowires. *Appl Phys Lett* 102:223110-1-223110-5

9. Jauregui LA, Pettes MT, Rokhinson LP, Shi L, Chen YP (2016) Magnetic field-induced helical mode and topological transitions in a topological insulator nanoribbon. *Nat Nanotechnol* 11:345–351
10. Bachtold Adrian, Strunk Christoph, Salvétat Jean-Paul, Bonard Jean-Marc, Forro Laszlo, Nussbaumer Thomas, Schonenberger Christian (1999) Aharonov–Bohm oscillations in carbon nanotubes. *Nature* 397:673–675
11. Hansen AE, Kristensen A, Pedersen S, Sorensen CB, Lindelof PE (2011) Mesoscopic decoherence in Aharonov–Bohm rings. *Phys Rev B* 64:0453271–045327-5
12. Huang SM, Wang Pin-Chun, Lin Chien, You Sheng-Yu, Lin Wei-Cheng, Lin Lin-Jie, Yan You-Jih, Yu Shih-Hsun, Chou MC (2018) The Aharonov–Bohm oscillation in the BiSbTe₃ topological insulator macroflake. *Appl Phys Lett* 112:203103-1–1203103-4
13. Huang ShiuMing, Huang Shih-Jhe, Yan You-Jih, Yu Shih-Hsun, Chou Mitch, Yang Hung-Wei, Chang Yu-Shin, Chen Ruei-San (2017) Extremely high-performance visible light photodetector in the Sb₂SeTe₂ nanoflake. *Sci Rep* 7:45413-1–45413-7
14. Huang SM, Yan YJ, Yu SH, Chou M (2017) Thickness-dependent conductance in Sb₂SeTe₂ topological insulator nanosheets. *Sci Rep* 7:1896-1–1896-7
15. Huang ShiuMing, Huang Shih-Jhe, Hsu Ching, Wadekar ParitoshV., Yan You-Jih, Yu Shih-Hsun, Chou Mitch (2017) Enhancement of carrier transport characteristic in the Sb₂SeTe₂ topological insulator nanosheets by N₂ adsorption. *Sci Rep* 7:5133-1–5133-8
16. Huang Shiu-Ming, Huang Shih-Jhe, Yan You-Jih, Yu Shih-Hsun, Chou Mitch, Yang Hung-Wei, Chang Yu-Shin, Chen Ruei-San (2017) Highly responsive photoconductance in a Sb₂SeTe₂ topological insulator nanosheet at room temperature. *RSC Adv* 7:39057–39062
17. Zhang SX, McDonald RD, Shekhter A, Bi ZX, Li Y, Jia QX, Picraux ST (2012) Magneto-resistance up to 60 Tesla in topological insulator Bi₂Te₃ thin films. *Appl Phys Lett* 101:202403-1–202403-5
18. Wang Z, Yang L, Zhao XT, Zhang ZD, Gao XuanPA (2015) Linear magnetoresistance versus weak antilocalization effects in Bi₂Te₃. *Nano Research* 8:2963–2969
19. Wang X, Du Y, Dou S, Zhang C (2012) Room Temperature Giant and Linear Magnetoresistance in Topological Insulator Bi₂Te₃ Nanosheets. *Phys Rev Lett* 108:266806-1–266806-5
20. Wang ZH, Yang L, Li XJ, Zhao XT, Wang HL, Zhang ZD, Gao XuanPA (2014) Granularity Controlled Nonsaturating Linear Magnetoresistance in Topological Insulator Bi₂Te₃ Films. *Nano Lett* 14:6510–6514
21. Barua S, Rajeev KP, Gupta AK (2015) Evidence for topological surface states in metallic single crystals of Bi₂Te₃. *J Phys Condens Matter* 27:015601-1–015601-10
22. Qu DX, Hor YS, Xiong Jun, RJ Cava, Ong NP (2010) Quantum oscillations and hall anomaly of surface states in the topological insulator Bi₂Te₃. *Science* 329:821–824
23. Assaf BA, Cardinal T, Wei P, Katmis F, Mooder JS, Heiman D (2013) Linear magnetoresistance in topological insulator thin films: Quantum phase coherence effects at high temperatures. *Appl Phys Lett* 102:012102-1–012102-4
24. Tang H, Liang D, Qiu RL, Gao XP (2011) Two-Dimensional Transport-Induced Linear Magneto-Resistance in Topological Insulator Bi₂Se₃ Nanoribbons. *ACS Nano* 5:7510–7516
25. Yan Y, Wang L-X, Yu D-P, Liao Z-M (2013) Large magnetoresistance in high mobility topological insulator Bi₂Te₃. *Appl Phys Lett* 103:033106-1–033106-4
26. He HT, Liu HC, Li BK, Guo X, Xu ZJ, Xie MH, Wang JN (2013) Disorder-induced linear magnetoresistance in (221) topological insulator Bi₂Te₃ films. *Appl Phys Lett* 103:031606-1–031606-4
27. He H, Li B, Liu H, Guo X, Wang Z, Xie M, Jiannong W (2012) High-field linear magneto-resistance in topological insulator Bi₂Te₃ thin films. *Appl Phys Lett* 100:032105-1–032105-3
He H, Li B, Liu H, Guo X, Wang Z, Xie M, Jiannong W
28. Hsiung TC, Mou CY, Lee TK, Chen YY (2015) Surface-dominated transport and enhanced thermoelectric figure of merit in topological insulator Bi_{1.5}Sb_{0.5}Te_{1.7}Se_{1.3}. *Nanoscale* 7:518–523
29. He X, Guan T, Wang X, Feng B, Cheng P, Chen L, Li Y, Kehui W (2012) Highly tunable electron transport in epitaxial topological insulator (Bi_{1-x}Sb_x)₂Te₃ thin films. *Appl Phys Lett* 101:123111-1–123111-5
30. Leea P-C, Huanga Y-C, Chiena CH, Chiu FY, Chen YY, Harutyunyan SR (2015) A comparative study of size-dependent magnetoresistance and Hall resistance of Sb₂Te₃ nanoflakes. *Physica B* 459:12–15
31. Wang K, Draf D, Petrovic C (2014) Large magnetothermopower and Fermi surface reconstruction in Sb₂Te₂Se. *Phys Rev B* 89:125202-1–125202-6
32. Huang SM, Yu SH, Chou M (2016) The linear magnetoresistance from surface state of the Sb₂SeTe₂ topological insulator. *J Appl Phys* 119:245110-1–245110-5
33. Huang SM, Yu SH, Chou M (2016) The large linear magnetoresistance in Sb₂SeTe₂ single crystal with extremely low mobility. *Mater Res Express* 3:126101-1–126101-5
34. Parish MM, Littlewood PB (2003) Non-saturating magnetoresistance in heavily disordered semiconductors, (London)
35. Xiang FX, Wang XL, Dou SX Transport evidence for the coexistence of the topological surface state and a two-dimensional electron gas in BiSbTe₃ topological insulator. [Arxiv.org/pdf/1404.7572](https://arxiv.org/pdf/1404.7572)
36. Camino FE, Zhou W, Goldman VJ (2005) Aharonov–Bohm electron interferometer in the integer quantum Hall regime. *Phys Rev B* 72:155313-1–155313-6
37. van Wees BJ, Kouwenhoven LP, Harmans CJPM, Williamson JG, Timmering CE, Broekaart MEI, Foxon CT, Harris JJ (1989) Observation of zero-dimensional states in a one-dimensional electron interferometer. *Phys Rev Lett* 62:2523–2526
38. Goldman VJ, Karakurt I, Liu J, Zaslavsky A (2001) Invariance of charge of Laughlin quasiparticles. *Phys Rev B* 64:085319-1–085319-5
39. Camino FE, Zhou W, Goldman VJ (2005) Aharonov–Bohm Superperiod in a Laughlin Quasiparticle Interferometer. *Phys Rev Lett* 95:246802-1–246802-4
40. Goldman VJ, Su B (1995) Resonant Tunneling in the Quantum Hall Regime: Measurement of Fractional Charge. *Science* 267:1010–1012
41. Zhang Yiming, McClure DT, Levenson-Falk EM, Marcus CM, Pfeiffer LN, WestKW (2009) Distinct signatures for Coulomb blockade and Aharonov–Bohm interference in electronic Fabry–Perot interferometers. *Phys Rev B* 79:241304-1–241304-4
42. Choi H, Jiang P, Godfrey MD, Kang W, Simon SH, Pfeiffer LN, West KW, Baldwin KW (2011) Aharonov–Bohm-like oscillations in Fabry–Perot interferometers. *New J Phys* 13:055007-1–055007-9
43. Choi HK, Sivan I, Rosenblatt A, Heiblum M, Umansky V, Mahalu D (2015) Robust electron pairing in the integer quantum hall effect regime. *Nat Commun* 6:7435-1–7435-7
44. Yu W, Jiang Y, Yang J, Dun ZL, Zhou HD, Jiang Z, Lu P, Pan W (2016) Quantum Oscillations at Integer and Fractional Landau Level Indices in Single-Crystalline ZrTe₅. *Sci Rep* 6:35357-1–35357-7
45. Qin Lai-Xiang, Pan Xin-Chen, Song Feng-Qi, Zhang Liang, Sun Zhang-Hao, Li Ming-Qiang, Peng Gao, Lin Ben-Chuan, HuangShiu-Ming, Zhu Rui, Xu Jun, Lin Fang, Lu Hai-Zhou, Yu Dapeng, Liao Zhi-Min (2018) Confined-path interference suppressed quantum correction on weak antilocalization effect in a BiSbTe₂ topological insulator. *Appl Phys Lett* 112:032102-1–032102-5

Publisher's Note

Springer Nature remains neutral with regard to jurisdictional claims in published maps and institutional affiliations.